RZ 3938 (# ZUR1703-103) 03/28/2017
Physical Sciences 35 pages

Research Report

Reorganization Energy Upon Charging a Single Molecule on an Insulator Measured by Atomic Force Microscopy

Shadi Fatayer[1], Bruno Schuler[1*], Wolfram Steurer[1], Ivan Scivetti[2#], Jascha Repp[3], Leo Gross[1], Mats Persson[2,4], Gerhard Meyer[1]

[1]IBM Research – Zurich, 8803 Rüschlikon, Switzerland

[2]Surface Science Research Centre, Department of Chemistry, University of Liverpool, United Kingdom

[3]Institute of Experimental and Applied Physics, University of Regensburg 93053 Regensburg, Germany

[4]Department of Applied Physics, Chalmers University of Technology, SE 41296, Göteborg, Sweden

*Current address: Molecular Foundry, Lawrence Berkeley National Laboratory, CA 94720, USA

[#]Current address: Daresbury Laboratory, Sc. Tech., Warrington, WA4 4AD, United Kingdom

This is the accepted version; the final version was published in *Nature Nanotechnology* **13(5)**, (2018): doi.org/10.1038/s41565-018-0087-1

Reorganization energy upon charging a single molecule on an insulator measured by atomic force microscopy

Shadi Fatayer,[1,*] Bruno Schuler,[1,†] Wolfram Steurer,[1] Ivan Scivetti,[2,‡] Jascha Repp,[3] Leo Gross,[1] Mats Persson,[2,4] and Gerhard Meyer[1]

[1]*IBM Research – Zurich, Säumerstrasse 4, 8803 Rüschlikon, Switzerland*

[2]*Surface Science Research Centre, Department of Chemistry, University of Liverpool, Liverpool, L693BX, United Kingdom*

[3]*Institute of Experimental and Applied Physics, University of Regensburg, 93053 Regensburg, Germany*

[4]*Department of Applied Physics, Chalmers University of Technology, SE 41296, Göteborg, Sweden*

(Dated: January 14, 2018)

Realizing single-electron transport between adsorbates on a non-conductive film is a key goal of molecular electronics [1–3]. Importantly, electron-transfer rates in molecular systems depend on a few fundamental parameters, such as distance between adsorbates, temperature [4–6] and in particular the Marcus reorganization energy [7]. This crucial parameter is the energy gain resulting from the distortion of the equilibrium nuclear geometry in the molecule and its environment upon charging. Here, we investigate redox reactions of naphthalocyanine molecules on a multilayered insulating NaCl film at 5 K. By employing the atomic force microscope as an ultra-low current meter based on single-electron detection we show that the differential conductance related to charge-state transitions can be measured. The hole reorganization energy of naphthalocyanine on NaCl is then quantified as (0.8 ± 0.2) eV. Density functional theory calculations corroborate the measured energy values and provide a detailed picture of the ionic and atomic relaxations upon individual charging. Our approach presents a versatile route to perform tunneling spectroscopy of single adsorbates on insulating substrates and provides fundamental insight into single-electron transport between molecules.

Electron transport in molecular devices, redox reactions and biological systems can be dominated by electron hopping [3–5], often studied within molecular nanostructures on top of insulating substrates to avoid charge leakage [8]. If the electronic states of the molecules are weakly coupled, charge transfer can be described using the semiclassical Marcus theory where the transfer rate is governed by the electron transfer integral, the temperature and the reorganization energy [7]. The latter influences the transfer rate exponentially, hence being decisive for the electron transfer. Not only do the geometry relaxations of the single molecule contribute to this energy, but also the relaxations of its surrounding can be relevant, as it occurs with dyes immersed in solvents [9, 10].

Realistic molecular devices are expected to be affected by the substrate upon charging. In fact, technologically relevant materials (e.g., SiO_2 and Al_2O_3) contribute to the reorganization energy [11]. Ionic substrates present an extreme case in this respect, because ionic relaxations can contribute a dominant fraction of the total reorganization energy [9, 12]. However, measuring reorganization energies of single molecules is very challenging, since it requires a technique that probes the molecular energy levels for well-defined charge-state

transitions. Ensemble-based techniques such as those used in electrochemistry [13] as well as optical [14, 15] and photoemission spectroscopies [16, 17] have been employed to measure the reorganization energy of molecules in solution, gas-phase and monolayer coverage on inert surfaces. Yet these techniques do neither allow for measurements at the relevant single molecule limit nor on insulating surfaces. Atomic force microscopy (AFM), with demonstrated single-charge sensitivity [18–22], atomic-scale spatial resolution [20] and the capability to operate on insulating films overcomes all these challenges. However, measurements of well-defined energy levels associated with charge transitions at the single-molecule limit on bulk insulators have, to date, not been achieved. The molecular energy levels are greatly influenced by the polarizability of its local environment, therefore the quantification of such effects is essential for the understanding of charge transport.

Here, we introduce a novel approach for measuring the hole reorganization energy E_{reorg} of a single-molecule adsorbed on an insulating film. The approach is based on a statistical analysis of single-electron transfer measurements between a metallic tip and naphthalocyanine (NPc), characterizing an outer-sphere reaction [13]. NPc is adsorbed on a 14 monolayer (ML) film supported by a Cu(111) substrate (see Figure S1). The constant frequency shift Δf image and adsorption model of NPc on NaCl are shown in Fig. 1a. Due to the thickness of the NaCl film, the electron tunneling through the film is quenched and the only possible electron transfer pathway is between the tip and the NPc, as sketched in Fig. 1b.

Fig. 1c depicts the AFM detection of a single electron transfer cycle involving a redox reaction of NPc ($NPc^0 \rightarrow NPc^+ \rightarrow NPc^0$). An electron is detached from the highest occupied molecular orbital (HOMO) by sweeping the sample voltage, starting from 0 V, to approximately -2.3 V. This corresponds to an oxidation of NPc^0 (denoted as ox^0). The electron transfer from the molecule to the tip is identified as a step in the frequency shift vs. sample voltage curve ($\Delta f(V)$) [20]. The horizontal shift of the extrapolated Kelvin probe parabolas (dashed lines) indicates that the molecule becomes positively charged. Subsequently, sweeping from negative voltages back to zero leads to the electron reattachment to NPc^+ from the tip, corresponding to a reduction of NPc^+ (denoted as red^+). Interestingly, red^+ occurs at a less negative voltage than ox^0, which results in a hysteretic behavior of the oxidation and reduction cycle.

The observed difference in the oxidation and reduction voltages is an effect of the reorganization energy, which can be understood from the corresponding single electron transfer

processes. These processes are the vertical (Franck-Condon) transitions ox^0 (red^+), occurring at fixed equilibrium geometry geo^0 (geo^+) of NPc^0 (NPc^+), as schematically displayed in Fig. 1d. The net energy change for the oxidation and reduction (the sum of the ox^0 and red^+ energy changes) equals the reorganization energy E_{reorg}. E_{reorg} is associated with the relaxations of the nuclear positions, i.e. the relaxation energies λ_+ and λ_0, also called heterogeneous reorganization energies [23].

Therefore, E_{reorg} is simply given by the energy difference between red^+ and ox^0 energy levels. Both levels can be probed by single electron tunneling at appropriate voltages. By starting with NPc^0 (NPc^+) and varying the sample voltage, the Fermi level of the metal tip aligns with the ox^0 (red^+) energy level and an electron tunnels to (from) the tip, as schematically represented in the electron energy diagram in Fig. 1e. In a free energy picture, the bias voltages applied will shift one specific charge state curve vertically with respect to the other. For the voltages associated with the ox^0 (red^+) energy level, the minimum in free energy of the NPc^0 (NPc^+) configuration intersects with the free energy curve of NPc^+ (NPc^0) and an electron is transferred to (from) the tip from (to) the molecule. Experimentally determining E_{reorg}, then, requires measuring the voltages associated with the red^+ and ox^0 energy levels. However, many repetitions of the charge transfer cycle reveal that the red^+ and ox^0 voltages vary between measurements (indicated as gray shading in Fig. 1c) and therefore requires a statistical analysis. These fluctuations occur because each transition reflects only one single tunneling event, being stochastic in nature. In addition, the ox^0 (red^+) levels are significantly broadened due to the strong coupling between an electron and the optical phonons in the ionic film and the zero-point fluctuations of their phonon coordinates at the low temperature of the experiment [12, 24, 25].

If both the electron detachment and reattachment processes could be observed in a steady-state situation then the corresponding current would already represent an average of the statistical tunneling process as, for example, in the electron detachment measurement of molecules on a bilayer NaCl with scanning tunneling spectroscopy [24]. In this case, the current is proportional to the corresponding transition rate. Here, however, we could not rely on such intrinsic self-averaging, but instead detect individual tunneling events. The transition rate can then be obtained from the average rate over many individual events. This new statistical approach to measure the rate of a specific charge state transition is summarized in Fig. 2 for transitions between the NPc^0 and NPc^+. First, the molecule

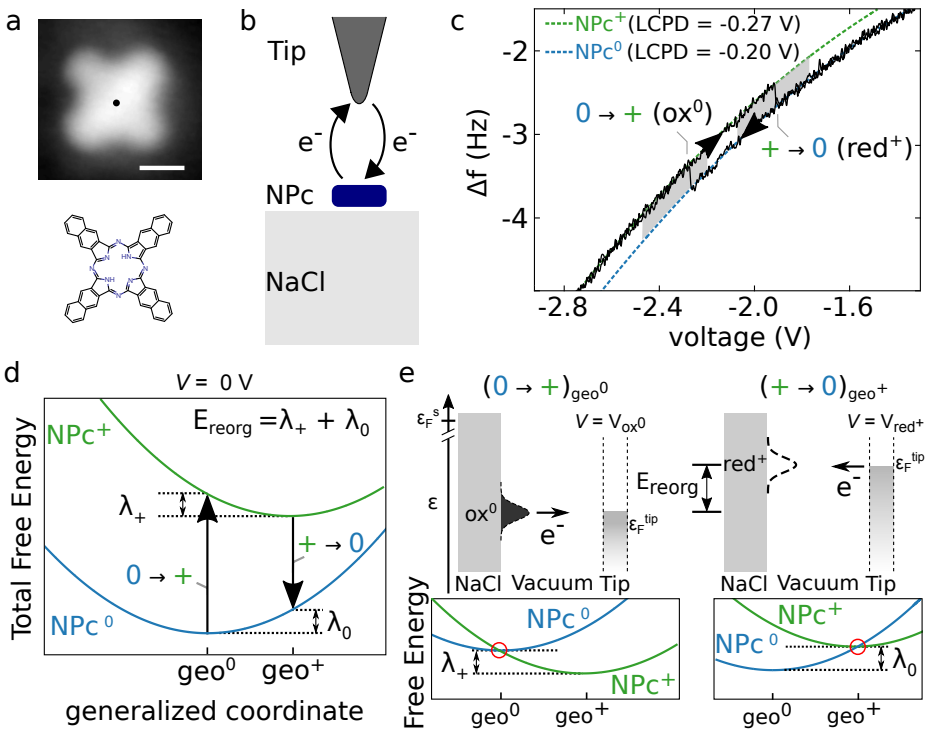

FIG. 1. AFM measurements of naphthalocyanine on a 14 ML NaCl film. **a,** AFM constant Δf image (Δf = -1.7 Hz, V = 1 V) of NPc on multilayer NaCl and corresponding chemical structure. The black dot indicates the spectrum position in **c**. The scale bar is 10 Å. **b,** Sketch of the experimental arrangement. Due to the thick NaCl film, electron transfer is only possible between tip and NPc, but not between Cu(111) and NPc. **c,** $\Delta f(V)$ spectrum recorded on a NPc molecule. Δf steps indicate an electron detachment from or reattachment to the highest occupied molecular orbital (HOMO). The dashed lines represent Kelvin parabolas of the neutral (NPc^0) and cation (NPc^+) species. Grey areas highlight the observed variation of voltages for electron detachment and reattachment. Note that the spectrum was recorded at a closer distance compared to other measurements in this publication to increase the transfer rate. **d,** Schematic of the total free energy curves for NPc^0 and NPc^+ with respect to the Fermi level of the tip at V = 0 V. The relaxation energy (also called heterogeneous reorganization energy) λ_+ is the energy difference between the energies of geo^0 and geo^+ along the NPc^+ potential energy curve. The relaxation energy λ_0 is the analogous for NPc^0. The hole reorganization energy E_{reorg} is the sum of λ_+ and λ_0. **e,** Electron energy ε diagrams corresponding to the sample voltages of electron detachment from NPc to the tip (ox^0, left) and electron reattachment from the tip to NPc (red^+, right). The difference in electron energies corresponds to the Marcus reorganization energy. In the bottom, the corresponding pictures for the total free energy at the respective sample voltage are depicted.

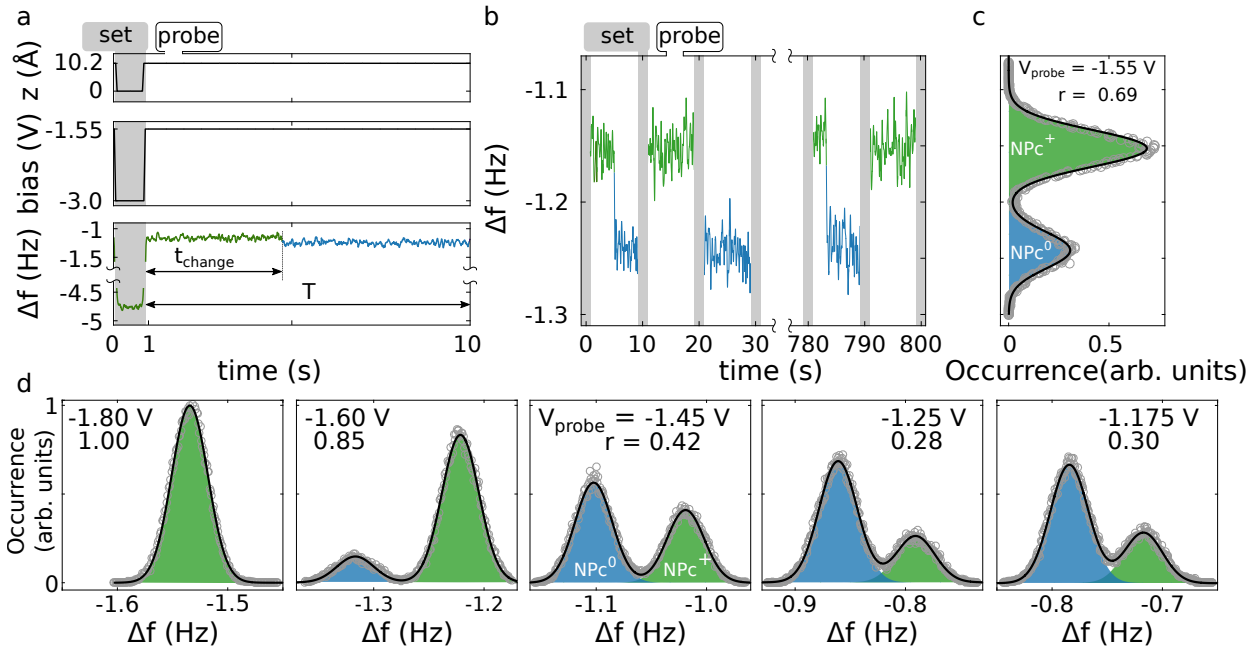

FIG. 2. Single-electron tunnel spectroscopy. **a,** Tip height z, sample voltage and $\Delta f(t)$ spectra for one probe cycle of electron reattachment to the cationic molecule. $\Delta f(t)$ indicates the measured residence time t_{change} in the initial set charge state. z_{probe} is the additional tip-surface distance with respect to the set point value. **b,** First three and last two of eighty measured probe traces $\Delta f(t)$ for $V_{\mathrm{probe}} = -1.55\,\mathrm{V}$. **c,** Histogram of the time integrated Δf of all probe traces measured for $V_{\mathrm{probe}} = -1.55\,\mathrm{V}$. Gaussians are fitted to the peaks. r denotes the fraction of the probe time in which the molecule remains in the set charge state (NPc^+, in this case) as obtained from the areas in the histogram (cf. Eq. (1)). **d,** Evolution and saturation of the Δf histograms for different V_{probe}.

was set to the desired charge state NPc^0 (NPc^+) by applying a voltage significantly above the red^+ (below the ox^0) voltage (see Fig. 1e) and by approaching the tip closely to the molecule at a distance $\mathrm{z_{set}}$, in order to provide a high tunneling rate. The electron transfer was then probed at appropriate values of voltage V_{probe} and tip height $\mathrm{z_{probe}}$. The latter was adjusted such that the charge transfer was detectable within the time-resolution of 0.1 s of our setup. The charge state was probed for a fixed probe time T of about 9 s and changes in the charge state were identified as steps in $\Delta f(t)$. Such a single 'set-probe' measurement is shown for the red^+ ($\mathrm{NPc}^+ \rightarrow \mathrm{NPc}^0$) in Fig. 2a. The statistical variation of the tunneling process was accounted for a record of 80 probe traces in total at a fixed V_{probe} (as shown

in Fig. 2b) obtained in four different sets of measurements. After each set of measurements the Δf feedback was enabled before measuring another set. The blue and green areas in the histograms shown in Fig. 2c,d correspond to the averaged residence times in the NPc^0 and NPc^+ state during the probe time T. The fraction r of the total probe time in which the molecule remains in the set charge state, at a certain V_{probe}, is given by

$$r = \frac{A_{\text{set}}}{A_{\text{set}} + A_{\text{final}}} = \frac{\left(1 - e^{-\Gamma T}\right)}{\Gamma T}. \tag{1}$$

Here A_{set} and A_{final} are the areas representing the averaged residence times during the probe time T of the initially set and the final charge states, respectively. These areas are obtained from the Δf histograms of all probe traces and exemplified in Fig. 2c in green and blue, respectively. The tunneling rate Γ is the inverse of τ, the lifetime of the set charge state at probing conditions (derivation details are in the Supplemental Information).

The evolution of r as a function of V_{probe} for the $NPc^+ \rightarrow NPc^0$ transition is shown in Fig. 2d. Starting from $r = 1$ at $V_{\text{probe}} = -1.8\,\text{V}$, indicating $\tau \gg T$, r decreases until it reaches a saturation value $r_{\text{sat}} \approx 0.3$ at a greater V_{probe}. z_{set} was defined as the tip height of the imaging setpoint above the molecule ($-1.7\,\text{Hz}$ at $1\,\text{V}$). The z_{probe} was $10.2\,\text{Å}$ from the imaging setpoint for probing the electron reattachment, corresponding to an effective tip–surface separation of about $22\,\text{Å}$ (details are in the Supplemental Information). An increased z_{probe} of $11.2\,\text{Å}$ was used for probing the electron detachment to ensure similar tunneling rates as measured for the electron reattachment while using lower V_{probe}.

Next we derive the single-electron differential tunneling rate to determine the voltages for electron detachment and reattachment from and to the HOMO of NPc (ox^0 and red^+). For every V_{probe}, the rate Γ can be derived from the experimentally determined $r(V_{\text{probe}})$ (see Eq. (1)). Γ can be interpreted as a single-electron tunneling current when multiplied by the elementary charge e. Consequently, the measured Gaussian-shaped differential conductance in the case of bilayer NaCl insulating films [12] translates to a Gaussian shape of the corresponding $d\Gamma/dV_{\text{probe}}$ in this experiment. Therefore, $\Gamma(V_{\text{probe}})$ is well fitted by an error function. The derivative of this fitting function is analogous to a differential conductance, the maximum of which indicates the ox^0 and red^+ voltages. In this analysis we assumed that the energy barrier is approximately constant for the voltage window of V_{probe}. The additional broadening due to the tip oscillation amplitude of $6\,\text{Å}$ is negligible (details are in the Supplemental Information).

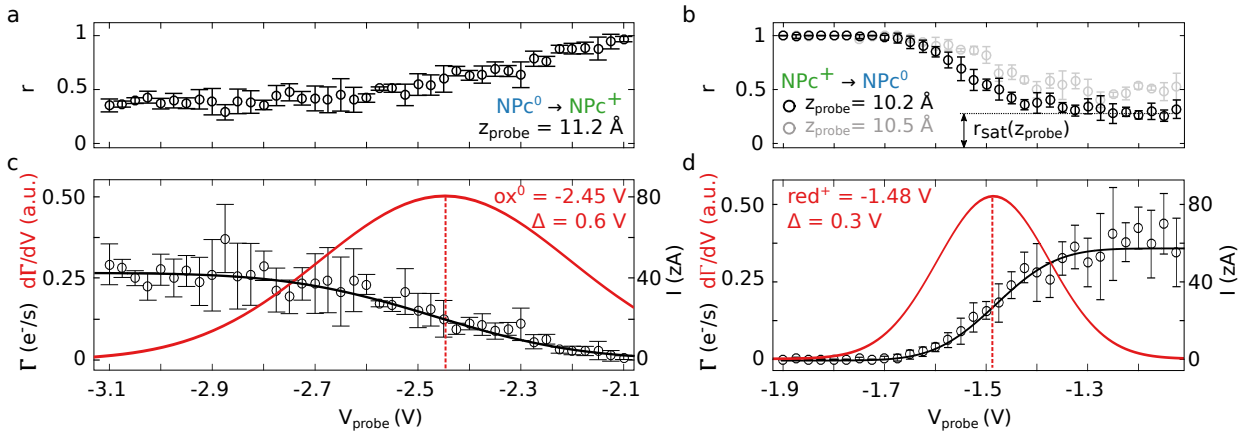

FIG. 3. Analysis of the charge-state transitions as a function of sample probe voltage V_{probe}. **a,c** HOMO — ox^0 ($NPc^0 \rightarrow NPc^+$). **b,d** HOMO — red^+ ($NPc^+ \rightarrow NPc^0$). **a** and **b** display the behavior of r as a function of V_{probe} (the saturation value r_{sat} along with the r results for a different z_{probe} are indicated in **b**). r denotes the fraction of the probe time in which the molecule remains in the set charge state as obtained from the areas in the histogram (cf. Eq. (1)). The error bars are the standard error of the mean r of each individual set of measurements of r. **c** and **d** represent the respective calculated tunneling rate Γ (the analogous value of tunneling current I is displayed in the right axis) along with the fitted error function (black line) and its derivative (red line) representing the respective orbital resonance. The peak positions ox^0 and red^+ (dashed vertical lines) and the full width at half maximum Δ of each peak are indicated in both graphs.

The results for the two different charge state transitions, $NPc^0 \rightarrow NPc^+$ and $NPc^+ \rightarrow NPc^0$, are displayed in Fig. 3 (the fitted Δf levels are shown in Figure S2). Fig. 3a,b show the evolution of $r(V_{probe})$ and their r_{sat} for the respective charge state transition. In Fig. 3b a second z_{probe} demonstrates that r_{sat} can be tuned by z_{probe}. The tunneling rate Γ and single-electron tunnel current I for each transition are shown in Fig. 3c,d and are well described by an error function (indicated by a black line). The ox^0 and red^+ voltages (dashed red lines in Fig. 3c and d) are (-2.44 ± 0.04) V and (-1.48 ± 0.05) V, respectively. The errors stem mainly from the uncertainty of r in determining the saturation region r_{sat} (error analysis is demonstrated in Figures S3–S5). The second z_{probe} measurement in Fig. 3b displayed a similar red^+ voltage level.

To obtain the oxidation and reduction energy levels from the corresponding voltages, the partial voltage drop across the NaCl dielectric film needs to be estimated. A calculation

using a finite element model of the tip and the insulator provides a voltage drop of $\approx$ 17 % across the insulating film (see Figure S6 and [26]). Accordingly, this correction yields ox^0 and red^+ energy levels of (-2.04 $\pm$ 0.15) eV and (-1.23 $\pm$ 0.10) eV, respectively. The absolute difference between these two energies is E_{reorg}, quantified as (0.81 $\pm$ 0.18) eV for NPc on NaCl. The uncertainty in the reorganization energy value is comparable to the errors obtained from photoelectron spectroscopy on molecular films [27].

The full width at half maximum of the ox^0 and red^+ voltage levels were found to be distinctly different, being (0.6 $\pm$ 0.1) V and (0.25 $\pm$ 0.13) V, respectively. For an explanation of the difference in line widths, the potential energy landscape of NPc^0 and NPc^+ on NaCl along with the tip induced polarization of the film need to be addressed. This complex task deserves further investigation. The peak position of the ox^0 level can be compared to scanning tunneling spectroscopy measurements of NPc on a NaCl bilayer [28]. The peak position for the bilayer (-1.7 V) is shifted upwards, the difference is discussed below. The peak width ($\approx$ 0.2 V) for the bilayer is smaller than the width reported here.

The measured values for the ox^0 and red^+ energy levels and the reorganization energy were corroborated by simulations based on density functional theory (DFT) of the film and the adsorbed molecule using a perfect conductor model of the metal support and a force field between the metal and the surface (see Methods for details). These energies were computed for NaCl thicknesses between 2 to 5 ML. Using finite-size scaling based on the asymptotic behaviour of these energies with the inverse number of NaCl monolayers N_l, the extrapolated values at 14 ML are -2.08 eV and -1.29 eV for the ox^0 and red^+ energy levels, respectively, and 0.79 eV for the hole reorganization energy (see Figure S7). These calculations are in good agreement with the corresponding experimental energies obtained above. However, the excellent agreement for the ox^0 and red^+ energy levels might be fortuitous because these energies involve a change of the charge state and, therefore, they are sensitive to the self-interaction error of the employed exchange-correlation functional in DFT. The measured upward shift of $\approx$ 0.3 eV of the ox^0 energy level for NPc on the bilayer NaCl compared to the 14 ML results is also in good agreement with the calculated value of 0.23 eV. This upward shift is predominantly caused by the image interaction with the metal surface (see Figure S7). At 14 ML, the calculated reorganization energy is dominated by the ionic polarization in the film. An extrapolation to $N_l = \infty$ increases the reorganization energy of NPc on 14 ML by only 0.06 eV. The intramolecular contribution to the hole reorganization energy is

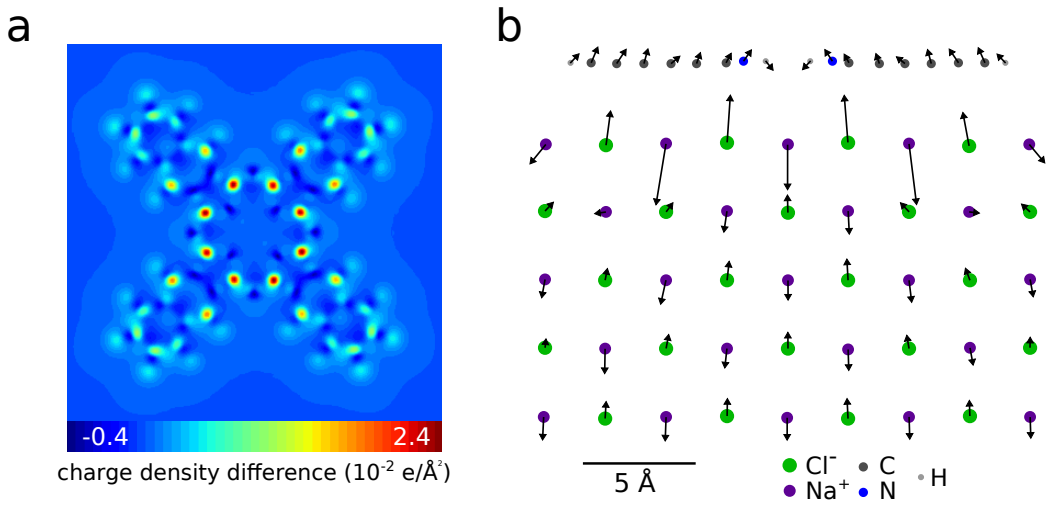

FIG. 4. DFT analysis of naphthalocyanine on NaCl(5 ML). **a,** 2D contour plot of the calculated charge density difference between $NPc^{+}_{geo^{+}}$ and $NPc^{0}_{geo^{+}}$ integrated outwards from the molecular plane to the vacuum region. **b,** Calculated atomic displacements of $NPc^{+}_{geo^{+}}$ with respect to $NPc^{0}_{geo^{0}}$. The map is the plane containing the non-polar direction of NaCl and along the center position of the imine nitrogens. The in-plane displacement vectors are magnified 40 times.

less than 3 %. A single image charge interaction model was used to estimate the influence of the metallic tip in the reorganization energy measurements. This estimate results in a small reduction of E_{reorg} of about 0.02 eV (see Figure S9).

The calculated charge density difference between $NPc^{+}_{geo^{+}}$ and $NPc^{0}_{geo^{+}}$ on NaCl(5 ML) is shown in Fig. 4a as a 2D contour plot of this density integrated outwards from the molecular plane to the vacuum region. This hole charge density is more or less delocalized over the molecule and is very similar to the corresponding density of NPc in the gas-phase (see Figure S8). This charge delocalization is consistent with the homogeneous ionic relaxation pattern of the 5 ML film upon charging which is shown in Fig. 4b. The major ionic response to the hole charge occurs in the NaCl surface layer, with the Na ions underneath the NPc macrocycle having the greatest displacements ($\approx$ 7.5 pm) reflecting a higher hole charge density in the macrocycle compared to the phenyl groups. The atoms in the subsurface layers show a similar displacement pattern but their displacements are significantly smaller than for the surface layer. The similar magnitudes of these displacements in the subsurface layers are due to the long-range electric field from the delocalized hole charge density. Despite this charge delocalization, the relative large reorganization energy can be reconciled by the

results of a simple dielectric model (details in the Supporting Information). Somewhat surprisingly, the molecule is displaced slightly upward ($\approx 2.0\,\mathrm{pm}$) upon charging.

In conclusion, we have directly measured the reorganization energy caused by the charging of a single molecule adsorbed on an insulating film using scanning probe microscopy. The method introduced here revolves around detecting single-electron transfer processes, based on the single-charge sensitivity of atomic force microscopy that allows us to measure transition rates that corresponds to currents in the zepto Ampere range. By applying this method to single NPc molecules on top of a multilayer NaCl film, the hole reorganization energy was obtained. The results were corroborated and analyzed by density functional theory calculations, in which the metal support of the multilayer film was treated implicitly. The experimental method can be extended to other ionic as well as to nonionic insulating films as well as other adsorbates, different charge state transitions and be performed at elevated temperatures. The methodology described here could also be applied to different AFM setups, provided conductive tips can be used. Quantification of the specific influence of the local environment on the reorganization energy of molecules and atoms on insulators can be readily achieved. The ability to measure reorganization energies at the atomic scale paves the way to quantify and predict single electron transfer processes between molecules on insulating films and opens up the prospects of tuning and manipulating their energy transfer [29].

In conclusion, we have directly measured the hole reorganization energy caused by the charging of a single naphthalocyanine molecule adsorbed on top an insulating NaCl film using scanning probe microscopy. Our method revolves around detecting single-electron transfer processes, based on the single-charge sensitivity of atomic force microscopy that allows us to measure transition rates that corresponds to currents in the zeptoampere range. We corroborated and analyzed our results by density functional theory calculations, in which the metal support of the multilayer film is treated implicitly. The experimental method can be extended to other insulating films (ionic and non-ionic) as well as other adsorbates, different charge state transitions and be performed at elevated temperatures; moreover, it could also be applied to different AFM setups, provided conductive tips can be used. Quantification of the specific influence of the local environment on the reorganization energy of molecules and atoms on insulators can be readily achieved. The ability to measure reorganization energies at the atomic scale is indispensable to quantify and predict single

electron transfer processes between molecules on insulating films and, in turn, tune and manipulate their energy transfer rates [29].

METHODS

STM and AFM measurements

Experiments were carried out with a combined scanning tunneling/atomic force microscope that utilizes a qPlus tuning fork sensor [30], which was operated in the frequency modulation mode [31] oscillating at 30.1 kHz. An oscillation amplitude of $A = 6$ Å was chosen to optimize the signal to noise ratio in detecting single charges. The microscope was operated under ultrahigh vacuum ($p \approx 10^{-11}$ mbar) and low temperature ($T \approx 5$ K) conditions. Voltages were applied to the sample. Positive height offsets used in z_{probe} refer to an increase in the tip–molecule distance. The tip is made of PtIr and has been indented and characterized on the Cu(111) surface to yield and ensure a purely metallic tip.

Sample preparation

The substrate consisted of a 14 monolayer thick NaCl film grown on Cu(111) (for details on the thickness determination see Supplemental Material and [32]). This insulating layer prevents tunneling between NPc and the Cu(111). Evaporation of a low quantity of NPc molecules on top of the surface resulted in a low estimated coverage of ≈ 60 molecules per 1000×1000 Å^2 with molecules mostly being isolated from each other. Therefore, charge transfer between molecules was inhibited [33]. As noted in [28], no tautomerization of the molecule can be identified while detaching an electron from the HOMO of NPc.

DFT calculations

The ox^0 and red^+ energy levels and the hole reorganization energy of a single NPc molecule adsorbed on a NaCl film supported by a Cu(111) substrate were computed using a new method implemented in VASP [34] which allows charged systems outside a metal

surface to be handled in a supercell geometry [35, 36]. In this method, the NaCl film and the adsorbed molecule were treated using DFT, whereas the support of the metals was described by a perfect conductor model and the residual interactions between the film and the metal were modelled by a simple force field. In this method the metal tip is not included.

In the calculations, the projector augmented wave (PAW) method [37] was used to describe the electron-ion interaction with a plane wave cut-off energy of 400 eV. The electronic exchange and correlation effects were treated using the optB86b version of the van der Waals (vdW) density functional [38–41]. The NaCl film was modelled by a slab with a [001] termination of bulk NaCl and 8×8 repetitions of the primitive surface unit cell, which corresponds to 64 Na and 64 Cl atoms in each layer. The film forms an incommensurate structure on the Cu(111) surface and as suggested by experiments for a bilayer [42], surface lattice constants of 3.895 Å, 3.91 Å, 3.93 Å and 3.94 Å were used in the calculations for the free-standing films with thicknesses between 2 to 5 ML, respectively. The same force field was used as for Cu(100), whereas the work function difference of 0.26 eV between NaCl films on Cu(100) and Cu(111), which only affects the transition energies, was accounted for by increasing the effective work function by the same amount. The cation was obtained by constraining the film and the molecule to have a net charge of $+1e$. The lateral electrostatic interactions between the periodic images were compensated by using a dipole-dipole correction scheme described in Ref. [43]. All atoms in the molecule and the NaCl film were allowed to relax during structural relaxations until the forces were less than 0.02 eV/Å. The Na site was found to be the most stable site of the adsorbed NPc molecule and the long axis of the molecule was oriented along $[1\bar{1}0]$ directions. The calculated adsorption energy of NPc on the NaCl trilayer is 5.04 eV, corresponding to about 60 meV per atom in accordance with the scaling of the physisorption interaction with molecular size [44]. The ox^0 and red^+ energy levels are given by the vertical transition energies,

$$\varepsilon_{\mathrm{ox}^0} = E(\mathrm{NPc}^0_{\mathrm{geo}^0}) - E(\mathrm{NPc}^+_{\mathrm{geo}^0}) \tag{2}$$

$$\varepsilon_{\mathrm{red}^+} = E(\mathrm{NPc}^0_{\mathrm{geo}^+}) - E(\mathrm{NPc}^+_{\mathrm{geo}^+}) \tag{3}$$

where the subscripts "geo^0" and "geo^+" refer to the equilibrium geometries of the neutral and positively charged systems, respectively. Note that in the calculation of the energy of

NPc^+ the electron is detached to the Fermi level of the tip. The calculated reorganization energy λ is then simply given by,

$$\lambda = \varepsilon_{\mathrm{red}^+} - \varepsilon_{\mathrm{ox}^0}. \tag{4}$$

The data that support the results within this paper and other findings of this study are available from the corresponding author upon reasonable request.

* sfa at zurich.ibm.com

† Current address: Molecular Foundry, Lawrence Berkeley National Laboratory, California 94720, USA

‡ Current address: Daresbury Laboratory, Sc. Tech., Warrington, WA4 4AD, United Kingdom

[1] Ch. Joachim, J. K. Gimzewski, and A. Aviram, "Electronics using hybrid-molecular and mono-molecular devices," Nature **408**, 541–548 (2000).

[2] M. Ratner, "A brief history of molecular electronics," Nature Nanotechnology **8**, 378–381 (2013).

[3] N. J. Tao, "Electron transport in molecular junctions," Nature Nanotechnology **1**, 173–181 (2006).

[4] C. C. Moser, J. M. Keske, K. Warncke, R. S. Farid, and P. L. Dutton, "Nature of biological electron transfer," Nature **355**, 796–802 (1992).

[5] D. M. Adams, L. Brus, Ch. E. D. Chidsey, S. Creager, C. Creutz, Ch. R. Kagan, P. V. Kamat, M. Lieberman, S. Lindsay, R. A. Marcus, R. M. Metzger, M. E. Michel-Beyerle, J. R. Miller, M. D. Newton, D. R. Rolison, O. Sankey, K. S. Schanze, J. Yardley, and X. Zhu, "Charge Transfer on the Nanoscale: Current Status," The Journal of Physical Chemistry B **107**, 6668–6697 (2003).

[6] W. Haiss, C. Wang, I. Grace, A. S. Batsanov, D. J. Schiffrin, S. J. Higgins, M. R. Bryce, C. J. Lambert, and R. J. Nichols, "Precision control of single-molecule electrical junctions," Nature Materials **5**, 995–1002 (2006).

[7] R. A. Marcus, "Electron transfer reactions in chemistry. Theory and experiment," Reviews of Modern Physics **65**, 599–610 (1993).

[8] K. Moth-Poulsen and T. Bjornholm, "Molecular electronics with single molecules in solid-state devices," Nature Nanotechnology **4**, 551–556 (2009).

[9] V. Vaissier, P. Barnes, J. K., and J. Nelson, "Influence of polar medium on the reorganization energy of charge transfer between dyes in a dye sensitized film," Physical Chemistry Chemical Physics **15**, 4804 (2013).

[10] B. S. Brunschwig, S. Ehrenson and N. Sutin, "Solvent reorganization in optical and thermal electron-transfer processes," The Journal of Physical Chemistry **90**, 3657–3668 (1986).

[11] F. Manke, J. M. Frost, V. Vaissier, J. Nelson and P. R. F. Barnes, "Influence of a nearby substrate on the reorganization energy of hole exchange between dye molecules," Physical Chemistry Chemical Physics **17**, 7345 (2015).

[12] J. Repp, G. Meyer, S. Paavilainen, F. E. Olsson, and M. Persson, "Scanning Tunneling Spectroscopy of Cl Vacancies in NaCl Films: Strong Electron-Phonon Coupling in Double-Barrier Tunneling Junctions," Physical Review Letters **95** (2005).

[13] A. L. Eckermann D. J. Feld, J. A. Shaw and T. J. Meade, "Electrochemistry of redox-active self-assembled monolayers," Coordination Chemistry Reviews **254**, 1769–1802 (2010).

[14] R. L. Blackbourn and J. T. Hupp, "Probing the molecular basis of solvent reorganization in electron-transfer reactions," The Journal of Physical Chemistry **92**, 2817–2820 (1988).

[15] J. L. Bredas and G. B. Street, "Polarons, bipolarons, and solitons in conducting polymers," Accounts of Chemical Research **18**, 309–315 (1985).

[16] N. E. Gruhn, D. A. da Silva Filho, T. G. Bill, M. Malagoli, V. Coropceanu, A. Kahn, and J. L. Bredas, "The Vibrational Reorganization Energy in Pentacene: Molecular Influences on Charge Transport," Journal of the American Chemical Society **124**, 7918–7919 (2002).

[17] S. Duhm, Q. Xin, S. Hosoumi, H. Fukagawa, K. Sato, N. Ueno, and S. Kera, "Charge Reorganization Energy and Small Polaron Binding Energy of Rubrene Thin Films by Ultraviolet Photoelectron Spectroscopy," Advanced Materials **24**, 901–905 (2012).

[18] R. Stomp, Y. Miyahara, S. Schaer, Q. Sun, H. Guo, P. Grutter, S. Studenikin, P. Poole, and A. Sachrajda, "Detection of Single-Electron Charging in an Individual InAs Quantum Dot by Noncontact Atomic-Force Microscopy," Physical Review Letters **94** (2005).

[19] E. Bussmann and C. C. Williams, "Single-electron tunneling force spectroscopy of an individual electronic state in a nonconducting surface," Applied Physics Letters **88**, 263108 (2006).

[20] L. Gross, F. Mohn, P. Liljeroth, J. Repp, F. J. Giessibl, and G. Meyer, "Measuring the

Charge State of an Adatom with Noncontact Atomic Force Microscopy," Science **324**, 1428–1431 (2009).

[21] A. Roy-Gobeil, Y. Miyahara, and P. Grutter, "Revealing Energy Level Structure of Individual Quantum Dots by Tunneling Rate Measured by Single-Electron Sensitive Electrostatic Force Spectroscopy," Nano Letters **15**, 2324–2328 (2015).

[22] Y. Miyahara, A. Roy-Gobeil, and P. Grutter, "Quantum state readout of individual quantum dots by electrostatic force detection," Nanotechnology **28**, 064001 (2017).

[23] K. H. Bevan, "Electron transfer from the perspective of electron transmission: Biased non-adiabatic intermolecular reactions in the single-particle picture," The Journal of Chemical Physics **146**, 134106 (2017).

[24] J. Repp, G. Meyer, S. M. Stojkovic, A. Gourdon, and Christian Joachim, "Molecules on Insulating Films: Scanning-Tunneling Microscopy Imaging of Individual Molecular Orbitals," Physical Review Letters **94** (2005).

[25] J. Jortner, "Temperature dependent activation energy for electron transfer between biological molecules," The Journal of Chemical Physics **64**, 4860 (1976).

[26] R. M. Feenstra, "Electrostatic potential for a hyperbolic probe tip near a semiconductor," Journal of Vacuum Science & Technology B: Microelectronics and Nanometer Structures **21**, 2080 (2003).

[27] S. Kera and N. Ueno, "Photoelectron spectroscopy on the charge reorganization energy and small polaron binding energy of molecular film," J. Electron Spectrosc. Relat. Phenom. **204**, 2-11 (2015).

[28] P. Liljeroth, J. Repp, and G. Meyer, "Current-Induced Hydrogen Tautomerization and Conductance Switching of Naphthalocyanine Molecules," Science **317**, 1203–1206 (2007).

[29] H. Imada, K. Miwa, M. Imai-Imada, S. Kawahara, K. Kimura, and Y. Kim, "Real-space investigation of energy transfer in heterogeneous molecular dimers," Nature **538**, 364–367 (2016).

[30] F. J. Giessibl, "High-speed force sensor for force microscopy and profilometry utilizing a quartz tuning fork," Applied Physics Letters **73**, 3956 (1998).

[31] T. R. Albrecht, P. Grutter, D. Horne, and D. Rugar, "Frequency modulation detection using high-Q cantilevers for enhanced force microscope sensitivity," Journal of Applied Physics **69**, 668 (1991).

[32] W. Steurer, L. Gross, and G. Meyer, "Local thickness determination of thin insulator films via localized states," Applied Physics Letters **104**, 231606 (2014).

[33] W. Steurer, S. Fatayer, L. Gross and G. Meyer, "Probe-based measurement of lateral single-electron transfer between individual molecules," Nature Communications **6**, 8353 (2015).

[34] G. Kresse and D. Joubert, "From ultrasoft pseudopotentials to the projector augmented-wave method," Phys. Rev. B **59**, 1758 (1999).

[35] I. Scivetti and M. Persson, "The electrostatic interaction of an external charged system with a metal surface: a simplified density functional theory approach," Journal of Physics: Condensed Matter **25**, 355006 (2013).

[36] I. Scivetti and M. Persson, "A simplified density functional theory method for investigating charged adsorbates on an ultrathin, insulating film supported by a metal substrate," Journal of Physics: Condensed Matter **26**, 135003 (2014).

[37] P. E. Blöchl, "Projector augmented-wave method," Phys. Rev. B **50**, 17953–17979 (1994).

[38] J. Klimeš, D. R. Bowler, and A. Michaelides, "Van der waals density functionals applied to solids," Phys. Rev. B **83**, 195131 (2011).

[39] M. Dion, H. Rydberg, E. Schröder, D. C. Langreth, and B. I. Lundqvist, "Van der waals density functional for general geometries," Phys. Rev. Lett. **92**, 246401 (2004).

[40] T. Thonhauser, Valentino R. Cooper, Shen Li, Aaron Puzder, Per Hyldgaard, and David C. Langreth, "Van der waals density functional: Self-consistent potential and the nature of the van der waals bond," Phys. Rev. B **76**, 125112 (2007).

[41] G. Román-Pérez and J. M. Soler, "Efficient implementation of a van der waals density functional: Application to double-wall carbon nanotubes," Phys. Rev. Lett. **103**, 096102 (2009).

[42] J. Repp, W. Steurer, I. Scivetti, M. Persson, L. Gross, and G. Meyer, "Charge-state-dependent diffusion of individual gold adatoms on ionic thin NaCl films," Phys. Rev. Lett. **117**, 146102 (2016).

[43] I. Scivetti, and M. Persson, "Frontier molecular orbitals of single molecules adsorbed on thin insulating films supported by a metal substrate: A simplified density functional theory approach," Journal of Physics: Condensed Matter **35**, 355002 (2017).

[44] J. Björk, F. Hanke, C.A. Palma, P. Samori, M. Cecchini, and M. Persson, "Adsorption of Aromatic and Anti-Aromatic Systems on Graphene through $\pi - \pi$ Stacking," J. Phys. Chem. Lett. **1**, 3407-3412 (2010).

ACKNOWLEDGMENTS

We thank Rolf Allenspach for comments. Financial support by the European Research Council (Advanced grant 'CEMAS' - agreement no. 291194 and Consolidator grant 'AMSEL' - agreement no. 682144), EU projects 'PAMS' (Contract. No. 610446) and Initial Training Network 'ACRITAS' (Contract No. 317348). The Leverhulme Trust (F/00 025/AQ) and the allocations of computer resources at Chadwick, The University of Liverpool are gratefully acknowledged. I.S. acknowledges CCP5 EPSRC EP/M022617/1 and SLA for funding.

AUTHOR CONTRIBUTIONS

S.F, W.S, J.R, L.G. and G.M designed the experiments. S.F., B.S., L.G. and G.M. performed the experiments. S.F. carried out the finite element simulations. M.P. and I.S. were responsible for the DFT calculations. All authors discussed the results and wrote the manuscript.

COMPETING INTERESTS

The authors declare no competing financial interests.

ADDITIONAL INFORMATION

Supplementary information is available in the online version of the paper. Reprints and permission information is available online at www.nature.com/reprints. Correspondence and requests for materials should be addressed to S.F.

Reorganization energy upon charging a single molecule on an insulator measured by atomic force microscopy

SUPPLEMENTAL MATERIAL

Shadi Fatayer,[1,*] Bruno Schuler,[1,†] Wolfram Steurer,[1] Ivan Scivetti,[2,‡] Jascha Repp,[3] Leo Gross,[1] Mats Persson,[2,4] and Gerhard Meyer[1]

[1]*IBM Research – Zurich, Säumerstrasse 4, 8803 Rüschlikon, Switzerland*

[2]*Surface Science Research Centre, Department of Chemistry, University of Liverpool, Liverpool, L693BX, United Kingdom*

[3]*Institute of Experimental and Applied Physics, University of Regensburg, 93053 Regensburg, Germany*

[4]*Department of Applied Physics, Chalmers University of Technology, SE 41296, Göteborg, Sweden*

(Dated: October 2, 2017)

THICKNESS DETERMINATION OF THE NACL FILM

The NaCl thickness determination was performed by counting the number of layers in an AFM image relative to the terrace where a chlorine vacancy was created. For the terrace with the chlorine vacancy, the thickness was obtained via the lifetime measurement (tunneling current) of a chlorine vacancy state [1]. The vacancy was created after the reorganization energy experiments to avoid any tip changes during the charge state transition experiments. The relative number of layers between different film thicknesses was obtained by counting the number of mono-atomic steps in an AFM image at constant Δf, as seen in Fig. 1 (a). The creation of a chlorine vacancy in a favorable region along with the current vs. distance spectroscopy allowed the determination of the saturation current (shown in Fig. 1 (b)). The saturation current is determined by the lifetime of the vacancy state and correlates with the layer thickness. In our experiments, the saturation current at 2.6 V was $\approx 0.8\,\mathrm{pA}$, as indicated in Fig. 1 (b), corresponding to a lifetime of 9 μs and a 7 ML thick film according to Ref. [1]. The film thickness of the measurement region for naphthalocyanine (NPc) was then obtained as being 14 ML by counting the number of layers compared to the thickness where this chlorine vacancy was created.

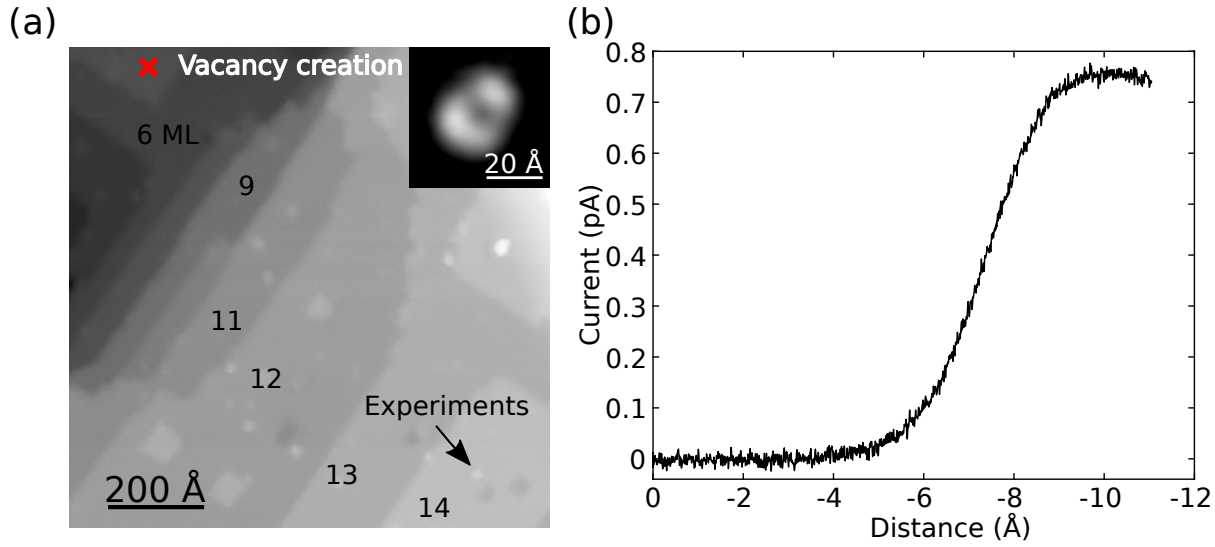

FIG. 1. **(a)** Constant Δf AFM overview image (Δf = -2 Hz, V = 1 V). The image covers the experimental region for NPc (black arrow) and the region used to create the chlorine vacancy (red cross). The inset shows an STM image of the created vacancy (set point of 4.2 V and 0.2 pA). **(b)** Tunneling current versus tip approach (distance) on top of the vacancy at a bias of 2.6 V. Tip approach of 0 Å corresponds to a STM set point of 4.2 V and 1 pA.

RELATION BETWEEN AVERAGE RESIDENCE TIME FRACTION r AND LIFETIME τ

Here, we derive the relation between the average residence time fraction r and the electron lifetime τ of a set state. Assuming a time independent tunneling probability between molecule and tip, for a molecule prepared in a particular set state at $t = 0$, the probability P_{set} to find the molecule in its original state will decrease exponentially with time as

$$P_{\mathrm{set}}(t_{\mathrm{probe}}) = e^{-t_{\mathrm{probe}}/\tau}. \tag{1}$$

where τ is the characteristic lifetime of the set state. This expression for the probability of the charge state change is similar to a radioactive decay. The lifetime of the initial charge state depends on the fixed voltage V_{probe} used to probe the molecule, because the tunneling probability is voltage dependent due to the voltage dependent density of states of the molecule.

The fraction r of the total probe time T, in which the molecule remains in the set state

equals $P_{\mathrm{set}}(t_{\mathrm{probe}})$ averaged over the time span $0 \leqslant t_{\mathrm{probe}} \leqslant T$, is given by,

$$r = \langle P_{\mathrm{set}}(t_{\mathrm{probe}}) \rangle_{0 \leqslant t_{\mathrm{probe}} \leqslant T} = \frac{1}{T} \int_0^T P_{\mathrm{set}}(t_{\mathrm{probe}})\, \mathrm{d}t_{\mathrm{probe}} = \frac{\tau}{T}(1 - e^{-T/\tau}). \tag{2}$$

The procedure to determine r and τ is explained in detail in the manuscript.

ESTIMATION OF THE TIP–SAMPLE DISTANCE

Previous studies, based on scanning tunneling microscopy with tip approach until mechanical contact with the sample is made, found that at a setpoint $I_0 = 2$ pA and $V_0 = 0.05$ V the tip–NaCl(2 ML) distance d_0 was roughly 5 Å [2] and that the exponential decay constant κ for the tunnel current was approximately 0.9 Å^{-1} based on Ref. [3]. Based on the exponential decay in tunneling current, we calculate the respective tip–sample distances using our setpoint of $I_1 = 40$ zA and $V_1 =$ -2.5 V and add the apparent height d_{apparent} of Naphthalocyanine on 2 ML NaCl imaged at its positive ion resonance, ≈ 5 Å. This allows the estimation of the tip–sample (tip to NaCl surface) distance $d_{\mathrm{estimated}}$ during the probing of the electron detachment from the HOMO as

$$d_{\mathrm{estimated}} = d_0 - \frac{1}{2\kappa} \ln\left(\left|\frac{I_1 V_0}{I_0 V_1}\right|\right) + d_{\mathrm{apparent}} \approx 22 \text{ Å}. \tag{3}$$

We attribute an error of 5 Å to $d_{\mathrm{estimated}}$ due to uncertainties related to the distances and κ cited above.

TIP OSCILLATION INFLUENCE IN THE TUNNELING RATE AND MEASURED VOLTAGE BROADENING OF THE OXIDATION AND REDUCTION LEVELS

The cantilever is oscillating during measurements with an amplitude of $A = 6$ Å, strongly affecting the instantaneous tunneling current. The current that is calculated from the observed switching rate therefore reflects an average current over the entire oscillation cycle. It is therefore important to keep the amplitude of oscillation the same for every complete set of measurement. As the vertical tip position affects not only the current but also the potential drop in the junction, the molecular levels also shift in energy with the oscillation of the tip. Hence, the oscillatory wiggling of the levels' positions may lead to an additional apparent broadening in the corresponding measurement.

This effect is expected to be very small, since the current is flowing predominantly at the cantilever's turnaround closest to the sample and therefore the molecular level is also predominantly probed at this particular position of the tip.

Quantitatively this can be expressed in a weight function, which reflects the relative contribution to the total current at the different tip positions. This weight function comprises the exponential decay of the current with distance as $I \propto \exp(-2\kappa\zeta)$, where the decay constant κ is about 0.9 Å^{-1} and ζ is the position of the oscillating tip. The cantilever moves slowly at the turnaround but fast at its center position, which gives rise to an additional contribution to the weight function of $1/(\pi\sqrt{A^2-\zeta^2})$ [4], where A is the amplitude of oscillation. Taking these two effects together, the relative weight of the current to the total average current is given by

$$w(\zeta) = \begin{cases} \frac{\exp(-2\kappa\zeta)}{J_0(2\kappa A)\pi\sqrt{A^2-\zeta^2}}, & \text{if } |\zeta| \leq A \\ 0, & \text{otherwise} \end{cases} \tag{4}$$

Here, $J_0(x)$ is the Bessel function of first kind that normalizes the weight function to $\int_{-A}^{A} w(\zeta)d\zeta = 1$. Evaluating this function for $A = 6$ Å and $\kappa = 0.9\,\text{Å}^{-1}$, one realizes that more than 90% of the current flows within a region of only 0.7 Å around the closest turnaround. Similarly, roughly 99.5% of the current flows within a region of only 2 Å around the closest turnaround. As the shift of energy levels for sub-Ångstrom tip displacement is irrelevant within the error margins (see above), the additional broadening from this effect can safely be neglected.

ERROR ESTIMATION

For every V_{probe}, 80 probe traces were measured in four probing sets (equal 20 probe traces), yielding four r values. The z feedback was open for the duration of each set. The arithmetic mean provides $r(V_{\text{probe}})$, whereas the standard deviation yields its uncertainty margin. These mean values and errors are plotted in Figure 3a,b of the main manuscript, as r vs. V_{probe}. Afterwards, the result is numerically converted from the fraction r to the lifetime of the electron τ based on equation 2. The corresponding error is propagated according to

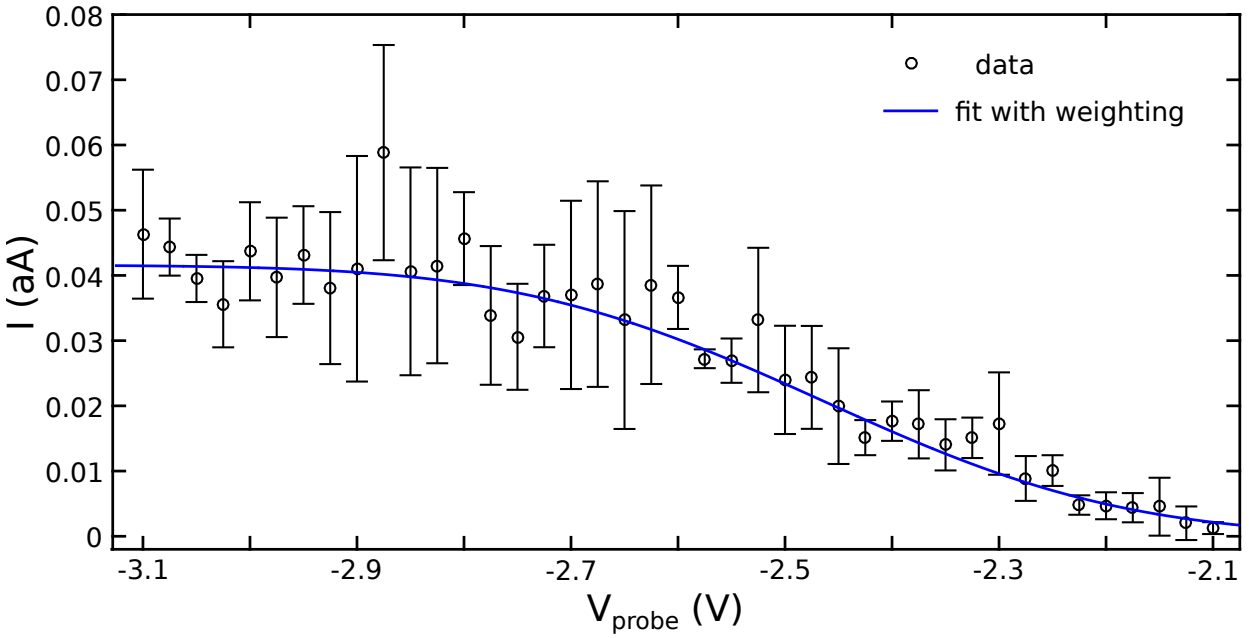

FIG. 2. Plot of I as a function of V_{probe} for the $\text{NPc}^0 \rightarrow \text{NPc}^+$ transition. The fitted error function possesses a weight proportional to the squared inverse of the current error.

$$\Delta\tau = \left(\frac{\Delta r}{\frac{1}{\mathrm{T}} - \frac{e^{\frac{-T}{\tau}}}{T} - \frac{e^{\frac{-T}{\tau}}}{\tau}} \right) \tag{5}$$

The next step is converting from τ to the tunneling rate Γ and the single-electron tunneling current I. Since τ, Γ and I are proportional or indirectly proportional to each other, their relative errors are all the same. The errors in I have a spread varying from 0.9 zA to 20 zA ($\Delta\Gamma$ analogously varies from 0.0056 e/s to 0.125 e/s). Next, we fit an error function curve to the I vs. V_{probe} behavior to numerically obtain the dI/dV_{probe} curve (also, $d\Gamma/dV_{\text{probe}}$) where the peak position and width are the important values obtained by the experiment. The fitting is performed with weights as the inverse of the error of each individual point, as shown in Fig. 2. The fitting results in a peak position of (-2.45 ± 0.04) V and a width of (0.57 ± 0.07) V.

To confirm the correctness of the error propagation, a Monte Carlo error analysis is performed. This consists in stochastically simulating the data and the error bars for a given charge state transition as in the real experiment. An example of a simulated data set is shown in Fig. 3. The peak position and width used are the same as the one fitted for the real data. Afterwards, we fit an error function (with weighting, as previously discussed)

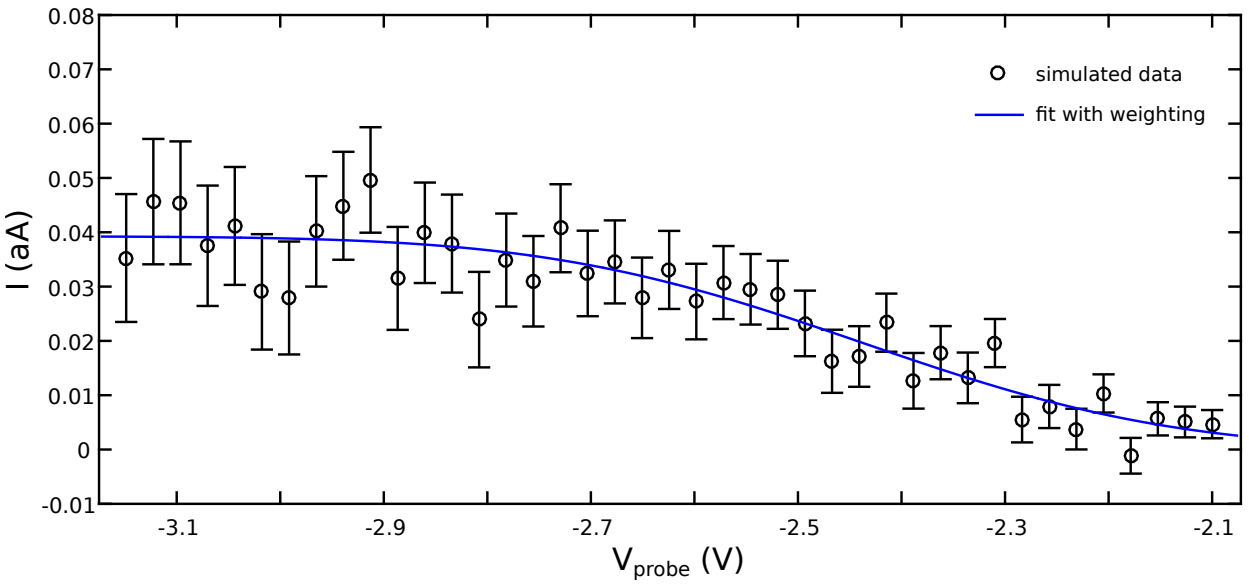

FIG. 3. Simulated data points of I as a function of V_{probe} for the $\text{NPc}^0 \rightarrow \text{NPc}^+$ transition.

and acquire the center and width of the dI/dV_{probe}. Different curves are generated with a random stochastic spread both in the simulated current and in the error bars. The stochastic spread in the simulations was chosen to closely mimic the experimentally observed spread in $r(V_{\text{probe}})$ The histograms for the fit results of 10000 different curves (each as in Fig. 3) are displayed in Fig. 4a,b and demonstrate the spread in the fitted dI/dV_{probe} peak position and width, respectively. The values obtained are (-2.44 ± 0.04) V and (0.6 ± 0.1) V for the peak position and width, respectively. This corroborates the former error estimations.
A similar error propagation procedure yiels a dI/dV_{probe} peak position of (-1.48 ± 0.05) V and width of (0.25 ± 0.13) V for the $\text{NPc}^+ \rightarrow \text{NPc}^0$ transition.

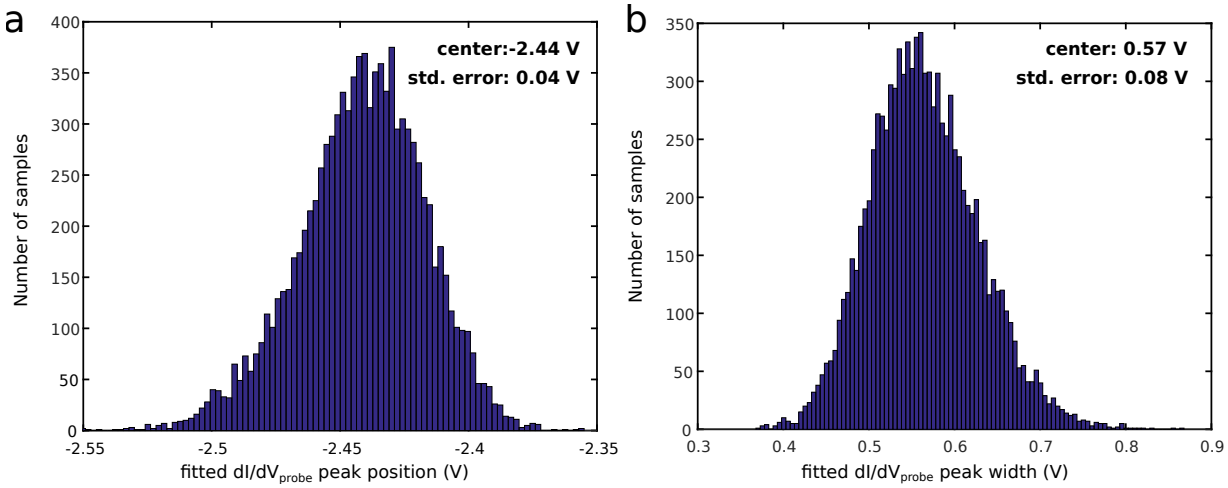

FIG. 4. Histogram of the spread in fitted peak position (a) and width (b) for 10000 simulated I vs. V_{probe} curves of the $\mathrm{NPc}^0 \rightarrow \mathrm{NPc}^+$ transition.

FITTED FREQUENCY SHIFT LEVELS FOR ELECTRON DETACHMENT AND REATTACHMENT

The fitted Δf levels for the electron detachment ($\mathrm{NPc}^0 \rightarrow \mathrm{NPc}^+$) and reattachment ($\mathrm{NPc}^+ \rightarrow \mathrm{NPc}^0$) are shown in Fig. 5. The curves recreate parabolas whose positive charge state has a local contact potential difference (LCPD) more negative in sample bias than the neutral charge state. The excellent parabolic fit of the voltage dependent Δf levels proves that the Gaussian fit routine is robust and that the Δf levels are associated with different charge states of the molecule, as indicated.

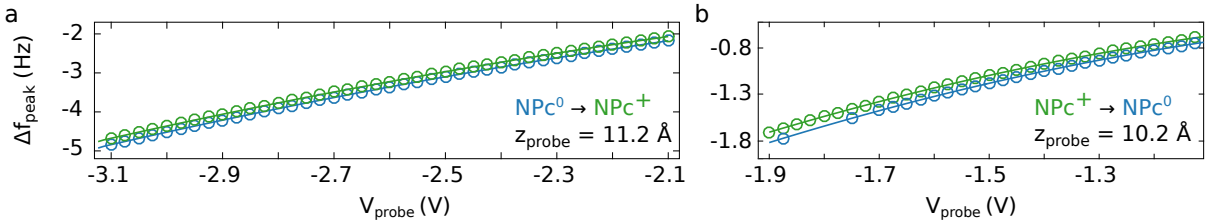

FIG. 5. Fitted Δf centers of the Δf histograms as a function of V_{probe} for each charge state transition performed in the main article. (a) electron detachment ($\mathrm{NPc}^0 \rightarrow \mathrm{NPc}^+$) and (b) electron reattachment ($\mathrm{NPc}^+ \rightarrow \mathrm{NPc}^0$). The positive (neutral) charge state is represented as green (blue) circles.

ESTIMATION OF VOLTAGE DROP ACROSS NACL

With respect to the electrostatic voltage drop, the tip-sample junction can be modeled in a simple 1D model as two planar capacitors connected in series. One capacitor corresponds to the vacuum region between tip and the surface of the NaCl film (C_{vac}), while the second capacitor corresponds to the NaCl film region (C_{NaCl}). These capacitances C_{x} are $\propto \epsilon_{\mathrm{x}}/d_{\mathrm{x}}$, where ϵ_{x} and d_{x} are the dielectric constant and spacing thickness of the region x, respectively. By assuming that the sample bias V_{bias} is applied between the tip and copper crystal, the bias voltage across the NaCl region V_{vac} is given by

$$V_{\mathrm{NaCl}} = \frac{V_{\mathrm{bias}}}{1 + \dfrac{\epsilon_{\mathrm{NaCl}} d_{\mathrm{vac}}}{\epsilon_{\mathrm{vac}} d_{\mathrm{NaCl}}}}. \tag{6}$$

In addition, we simulated the voltage drop for a more realistic 3D geometry of the tip. Here, we used a finite element method [5] due to its advantages in implementing the necessary geometrical and electrical constraints required to solve numerically the Laplace equation. We modeled our tip as a hyperboloid (geometry shown in Fig. 6a), following the work of Feenstra [6] and used relative dielectric constants of 1 and 6 for the vacuum and NaCl region, respectively. The metal support and the tip were treated as perfect conductors. In the simulations, we applied a voltage of 5 V, but its actual value does not change the relative voltage drop across the dielectric film. We used an uniform mesh sizing with 49919 nodes and 26370 elements. The voltage profile along the tip-sample system, shown in Fig. 6 (b), demonstrates that the deviation of this profile from the voltage profile of the 1D capacitor model increases with a sharper tip. Interestingly, the voltage drop across the NaCl film does not change significantly by varying the tip radius from 1000 Å (relative voltage drop of 20 percent in the NaCl) to 10 Å (relative voltage drop of 12 percent in the NaCl), while keeping the tip-sample distance constant. Therefore, we selected an intermediate radius value of 100 Å for our analysis of the reorganization energy of NPc with an error margin ranging from 10 Å to 1000 Å tip radii. Another important parameter is the tip-NaCl distance. Fig. 6 d depicts the relative voltage drop as a function of tip-NaCl distance both for a 100 Å radius tip and the 1D model. The tip-NaCl distance was estimated to be (22 ± 5) Å resulting in a relative voltage drop of (17 ± 3) % across the NaCl film. A slightly greater relative voltage drop of (18 ± 3) % was obtained for the electron reattachment measurements, due to a 1 Å increase in tip-NaCl distance.

The errors associated here account only for the tip-NaCl distance uncertainty. An additional error of approximately 4% is assumed for the tip radius, accounting on a conservative uncertainty of one order of magnitude for the tip radius (shown in Fig. 6 c). Therefore, considering uncertainties both in tip-NaCl distance and tip radius we obtain a relative voltage drop of (17 ± 5) % for electron detachment and (18 ± 5) % for electron reattachment.

Another point to consider is the relative voltage drop across the molecule. Since the adsorption height (obtained from DFT) is roughly the same as the step height of NaCl, we assumed an additional layer of NaCl to infer the upper limit of this effect as the dielectric of the molecule is not known. A simulation for a 15 ML NaCl film and a tip-sample height of approximately 19 Å yields a relative voltage drop of 19 %. Therefore, the maximum uncertainty in the voltage drop due to this effect is estimated to be approximately 2 %. By propagating all the errors enlisted here, the relative voltage drop across NaCl becomes (17 ± 6) % for electron detachment and (18 ± 6) % for electron reattachment.

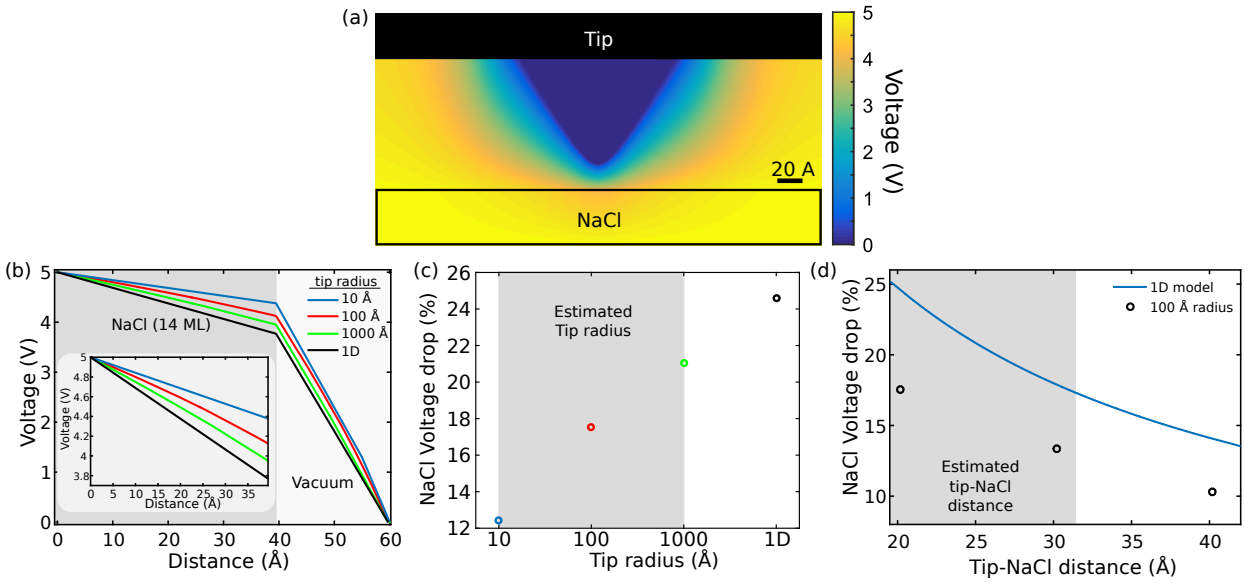

FIG. 6. **(a)** Schematics of the 3D model geometry and a contour plot of the voltage profile of a hyperbolic metallic tip above a 14 ML NaCl film. The tip radius is 10 Å, the vacuum gap is 20.2 Å and the voltage between tip and metallic surface is 5 V. **(b)** Voltage profile along the surface normal going through the tip apex for different tip radii (1000 Å, 100 Å and 10 Å) and the 1D capacitor model. **(c)** Relative voltage drop across the NaCl film as a function ot tip radius. Simulated results for a fixed vacuum gap of 20.2 Å and a 14 ML NaCl film. **(d)** Relative voltage drop across the NaCl film as a function of distance. Comparison between using a 100 Å radius tip in the finite element simulation and the 1D capacitor model.

REORGANIZATION ENERGY CALCULATION

In order to extrapolate oxidation ($\varepsilon_{\mathrm{ox}^0}$) and reduction ($\varepsilon_{\mathrm{red}^+}$) energies and reorganization energies (λ) (Eq.(2),(3) and (4) in main text) to 14 ML from their calculated values for 2 to 5 ML, we show them as a function of the inverse number of layers $1/N_l$ in Fig. 7. This extrapolation is based on the asymptotic behaviour of the energies with the film thickness, as suggested by the interaction of an external charge distribution with a dielectric film supported by a perfect conductor [7]. As shown in Fig. 7a, a linear extrapolation to $N_l \to \infty$ gives $\varepsilon_{\mathrm{ox}^0} \approx$ -2.08 eV, $\varepsilon_{\mathrm{red}^+} \approx$ -1.29 eV and $\lambda \approx 0.79$ eV for 14 ML. The importance of the lateral dipole correction is shown in the results for λ in Fig. 7 b. Without this correction, λ increases with N_l in accordance with the thickness dependence of the electrostatic energy of a planar capacitor with fixed surface charge density.

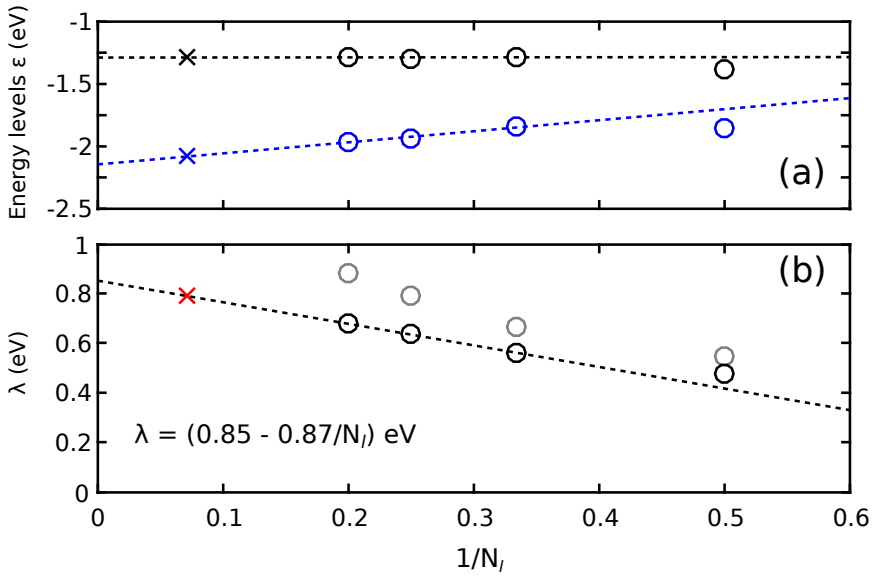

FIG. 7. Calculated (a) oxidation, $\varepsilon_{\mathrm{ox}^0}$, (blue circles) and reduction, $\varepsilon_{\mathrm{red}^+}$, (black circles) energy levels and (b) reorganization energy, λ (black circles) for NPc on a NaCl film supported by a Cu(111) surface as a function of the inverse number of monolayers $1/N_l$. The dashed lines are linear fits to the calculated energies from 3 to 5 ML and the crosses gives the extrapolated values at 14 ML ($N_l = 14$). The gray circles in (b) are the results for λ without lateral dipole-dipole corrections.

The magnitude of the calculated λ and its near linear decrease with $1/N_l$ (Fig.7) can be reconciled by the result from the simple dielectric model developed in Ref. [7] for a charged Pentacene molecule adsorbed on a NaCl film supported by a metal substrate. The charged molecule was modelled by a charged rectangular sheet at a vertical distance D from a dielectric film of relative dielectric constant ϵ_r and a thickness of $a_0 + N_l\Delta a$, where $a_0 = 0.84$ Å and $\Delta a = 2.81$ Å. The metal substrate is modelled by a perfect conductor. We set $D = 1.6$ Å, since the calculated adsorption height is 3.24 Å and the edge of the dielectic film is about 1.66 Å outside the surface plane [7]. In this model, $\lambda_+ = \lambda_-$ and λ_+ is given by the difference between the electrostatic interaction of the external charge with the unrelaxed and relaxed film. According to Eq. (B.7) in Ref. [7], λ_+ is then given asymptotically by,

$$\lambda_+ \asymp \left(\frac{\epsilon_{r0}-1}{\epsilon_{r0}+1} - \frac{\epsilon_{r\infty}-1}{\epsilon_{r\infty}+1)}\right)\frac{\tilde{Q}_{\rm F}^2}{16\pi\epsilon_0 D} + \left(\frac{4\epsilon_{r0}}{(\epsilon_{r0}+1)^2} - \frac{4\epsilon_{r\infty}}{(\epsilon_{r\infty}+1)^2}\right)\frac{\tilde{Q}_{\rm M}^2}{16\pi\epsilon_0(D+a_0+N_{\rm l}a)}, \text{for } N_{\rm l}\to\infty. \quad (7)$$

The first and second term on the right-hand side are obtained from the electrostatic interactions of the charged molecule with a semi-infinite dielectric material and the perfect conductor screened by the dielectric film, with and without ionic response, respectively. ϵ_{r0} is the static dielectric constant of the film and $\epsilon_{r\infty}$ is the optical dielectric constant. Here, the effective charges $\tilde{Q}_{F,M}$ take into account the lateral extension of the charge distribution of the charged molecule and are defined in Eq. (B.8) of Ref. [7]. In the case of a point charge with charge $\pm e$, $\tilde{Q}_{\rm F}^2 = \tilde{Q}_{\rm M}^2 = e^2$ but $\tilde{Q}_{\rm F,M}$ decreases for an increasing lateral extension of the charge distribution. In the case of the approximation of the hole charge distribution of the NPc molecule by an homogenously charged disc with a radius of 6 Å as indicated in Fig. 8a, $\tilde{Q}_{\rm F}^2 = 0.55e^2$ is a substantial reduction but much less so for $\tilde{Q}_{\rm F}^2 = 0.94 - 0.98e^2$ for $N_l = 2-5$, due to the much larger distance of the molecule from the metal surface than its distance from the dielectric film. As shown in Fig. 8b, the gas-phase charge density difference between NPc^0 and NPc^+ is similar to when NPc is adsorbed on NaCl.

Using the experimental bulk value of 5.62 for ϵ_{r0} [8] and the calculated value of 2.64 for $\epsilon_{r\infty}$ of the NaCl file [7] gives $\lambda_+ = 0.31$ eV for an infinitely thick film and a corresponding reorganization energy of $\lambda = 2\lambda_+ = 0.62$ eV. A value which can be reconciled by the calculated reorganization energy of about 0.85 eV at $N_l \to \infty$. Note that a dielectric model for the ionic and electronic response to an external charge distribution at such close distance is a rather crude approximation. Finally, the second term in Eq.(7) shows that λ decreases linearly in the asymptotic regime with $1/N_l$ in the asymptotic regime due to enhanced screening by the dielectric film when the ionic response is included.

This simple dielectric model can also reconcile the differences in the slopes of $\varepsilon_{\rm ox^0}$ and $\varepsilon_{\rm red^+}$ with $1/N_l$ (Fig.7). In the case of $\varepsilon_{\rm ox^0}$, this slope has the same magnitude but opposite sign as for the electrostatic interaction of the hole charge distribution with the unrelaxed film and is given by,

$$\frac{d\varepsilon_{\rm ox^0}}{dN_l^{-1}} = \frac{4\epsilon_{r\infty}}{(\epsilon_{r\infty}+1)^2}\frac{\tilde{Q}_{\rm M}^2}{16\pi\epsilon_0 a} \quad (8)$$

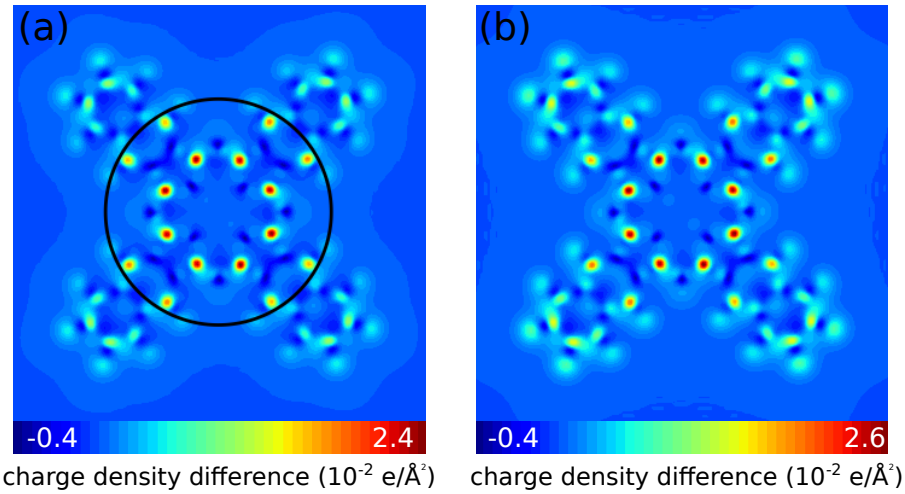

FIG. 8. Calculated charge density differences between (a) $NPc^{+}_{geo^{+}}$/NaCl(5ML) and $NPc^{0}_{geo^{+}}$/NaCl(5ML) and between (b) NPc^{+} and NPc^{0} in the gas phase. In the 2D contour plots, these density differences have been integrated outwards from the molecular plane to the vacuum region. The black circle in (a) indicates the homogeneously charged circular disc used in the dielectric model of the hole-charge distribution

Since $\varepsilon_{\mathrm{red}^{+}} = \varepsilon_{\mathrm{ox}^{0}} + 2\lambda_{+}$, the corresponding slope is according to equations (7) and (8) given by,

$$\frac{d\varepsilon_{\mathrm{red}^{+}}}{dN_l^{-1}} = \left(\frac{8\epsilon_{r0}}{(\epsilon_{r0}+1)^2} - \frac{4\epsilon_{r\infty}}{(\epsilon_{r\infty}+1)^2} \right) \frac{\tilde{Q}_{\mathrm{M}}^2}{16\pi\epsilon_0 a} \tag{9}$$

Using the values 2.64 and for $\epsilon_{r\infty}$ and ϵ_{r0}, respectively, one obtains that the slope should be about 3.5 times larger for $\varepsilon_{\mathrm{ox}^{0}}$ than for $\varepsilon_{\mathrm{red}^{+}}$.

As shown by the results in Fig. 7b, λ at $N_l = 14$ is only about 7 % less than its extrapolated value for an infinitely thick film. Furthermore, we find that the contribution to λ from intramolecular relaxations is small. Using the calculated equilibrium geometry of NPc^{0} on 3 ML and allowing only the ions in the film to relax for the equilibrium geometry of NPc^{+}, λ was found to decrease by about 0.020 eV, corresponding to a decrease of about 3 % of the calculated hole reorganization energy.

The contribution of the electrostatic interaction energy between the metallic tip and the adsorbed molecule on the reorganization energy has been estimated in a single image charge interaction model. The induced charge distribution of the adsorbed molecule in the absence of the tip has been modelled by a perpendicular dipole moment μ_0 and a point charge q_0 both located at the center of the molecule and a corresponding screening charge distribution

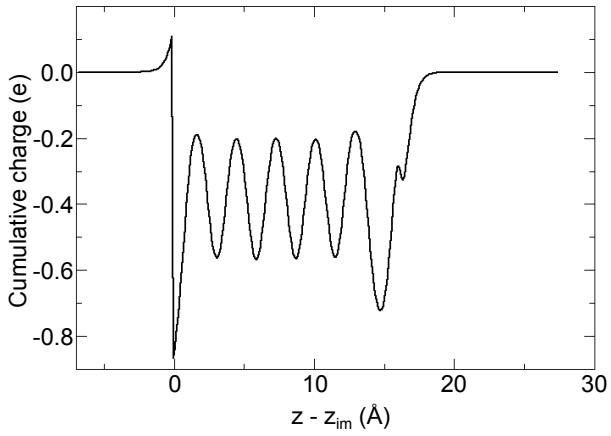

FIG. 9. Calculated cumulative charge $\Delta Q(z)$ of the laterally averaged charge density difference $\hat{\rho}(z)$ between $\mathrm{NPc}^{+}_{geo^0}$/NaCl(5 ML) and $\mathrm{NPc}^{0}_{geo^0}$/NaCl(5 ML) as a function of the perpendicular distance z. $\Delta Q(z) = \int_{-\infty}^{z} \hat{\rho}(z')dz'$ and z_{im} is the position of the image plane.

in the metal. μ_0 and q_0 for the adsorption of the molecule on 14 NaCl layers have been been estimated from the calculated perpendicular dipole moment μ of the induced charge distribution for adsorption of 4-5 layers based on the following asymptotic behaviour of μ with the distance L between the molecule and the image plane,

$$\mu(L) \asymp \mu_0 + q_0 L \ . \tag{10}$$

The resulting values of μ_0 and q_0 for the different neutral and positively charged states of the adsorbed molecule are shown in Table I.

The somewhat counterintuitive findings that $q_0 < e$ for NPc^{+} and also $q_0 \neq 0$ for NPc^{0} are both due to the dielectric polarization of the film. This polarization is illustrated by the calculated cumulative charge $\Delta Q(z)$ of the laterally averaged charge density difference between $\mathrm{NPc}^{+}_{geo^0}$ and $\mathrm{NPc}^{0}_{geo^0}$ in Fig. 9. The image charge $-e$ at the image plane is reduced in magnitude to about -$q_0(\mathrm{NPc}^{+}_{geo^0})$ - $q_0(\mathrm{NPc}^{0}_{geo^0})$ = -(0.25 - (-0.10))e = -0.35e by the charge at the metal-NaCl interface which is compensated by the charge at NaCl-molecule interface and the positively charged molecule. The oscillations in $\Delta Q(z)$ in the NaCl film are due to the dipolar polarizations of the NaCl layers. In a planar model of the tip, the single-image interaction energy $E_{\mathrm{im-tip}}$ of the induced charge distribution by the adsorbed molecule with

	$NPc^0_{geo^0}$	$NPc^+_{geo^0}$	$NPc^+_{geo^+}$	$NPc^0_{geo^+}$
μ_0 (eÅ)	1.96	3.03	2.94	-0.96
q_0 (e)	-0.10	0.25	0.09	-0.21
$E_{\mathrm{im-tip}}$ (meV)	-0.3	-15	-5	-6

TABLE I. Dipole moments, μ_0, and point charges, q_0, and single-image interaction energies, $E_{\mathrm{im-tip}}$, of different charge states of the adsorbed molecule on a 14ML film. The notation of these states is the same as in Equations (2) and (3) of the main manuscript.

the tip is given by,

$$\begin{aligned} E_{\mathrm{im-tip}} = & -\frac{q_0^2}{8\pi\epsilon_0}\left(\frac{1}{2d} - \frac{2}{2(d+L)} + \frac{1}{2d+4L}\right) \\ & -\frac{\mu_0^2}{4\pi\epsilon_0}\left(\frac{1}{8d^3} + \frac{2}{8(d+L)^3} + \frac{1}{8(2L+d)^3}\right) \\ & -\frac{\mu_0 q_0}{8\pi\epsilon_0}\left(\frac{2}{4d^2} - \frac{2}{4(d+2L)^2}\right), \end{aligned} \tag{11}$$

where d is the tip-molecule distance and $L = D + a_0 + N_l a$. Table I shows in the prevailing case of a 14 ML film, where $L = 41.7$ Å, and $d \approx 20$ Å, the calculated values of $E_{\mathrm{im-tip}}$ for the different neutral and positively charged states of the adsorbed molecule. According to Equations (2) and (3) of the main manuscript, the net contribution to the reorganization energy is then estimated to be (-15-(-5)-6-(-0.3) meV = -16 meV. That is, $\approx 2\%$ of the measured reorganization energy is related to tip image charges.

* sfa at zurich.ibm.com

† Current address: Molecular Foundry, Lawrence Berkeley National Laboratory, California 94720, USA

‡ Current address: Daresbury Laboratory, Sc. Tech., Warrington, WA4 4AD, United Kingdom

[1] W. Steurer, L. Gross, and G. Meyer, "Local thickness determination of thin insulator films via localized states," Applied Physics Letters **104**, 231606 (2014).

[2] L. Gross, F. Mohn, P. Liljeroth, J. Repp, F. J. Giessibl, and G. Meyer, "Measuring the Charge State of an Adatom with Noncontact Atomic Force Microscopy," Science **324**, 1428–1431 (2009).

[3] J. Repp, *Rastertunnelmikroskopie und spektroskopie an Adsorbaten auf Metall und Isolatoroberflächen*, PhD thesis. Freie Universität Berlin (2002).

[4] F. J. Giessibl "A direct method to calculate tip-sample forces from frequency shifts in frequency-modulation atomic force microscopy," Applied Physics Letters **78**, 123 (2001).

[5] ANSYS AIM, Release 17.0, Help System, ANSYS, Inc,.

[6] R. M. Feenstra, "Electrostatic potential for a hyperbolic probe tip near a semiconductor," Journal of Vacuum Science & Technology B: Microelectronics and Nanometer Structures **21**, 2080 (2003).

[7] I. Scivetti, and M. Persson, "Frontier molecular orbitals of single molecules adsorbed on thin insulating films supported by a metal substrate: A simplified density functional theory approach," Journal of Physics: Condensed Matter **35**, 355002 (2017).

[8] A. J. Dekker, *Solid State Physics* (Prentice-Hall, Englewood Cliffs, NJ, 1957).